Manuscript prepared for Atmos. Chem. Phys. Discuss.
with version 2014/07/29 7.12 Copernicus papers of the LaTeX class copernicus.cls.
Date: 30 January 2015

Quantifying contributions to the recent temperature variability in the tropical tropopause layer

W. Wang[1,2], **K. Matthes**[2,3], **and T. Schmidt**[4]

[1]Freie Universität Berlin, Institut für Meteorologie, Berlin, Germany
[2]GEOMAR Helmholtz-Zentrum für Ozeanforschung Kiel, Kiel, Germany
[3]Christian-Albrechts Universität zu Kiel, Kiel, Germany
[4]Helmholtz Zentrum Potsdam, Deutsches GeoForschungsZentrum (GFZ), Potsdam, Germany

Correspondence to: W. Wang (wuke.wang@fu-berlin.de)

Abstract

The recently observed variability in the tropical tropopause layer (TTL), which features an unexpected warming of 1.0 K over the past decade (2001–2011), is investigated with a number of sensitivity experiments from simulations with NCAR's CESM-WACCM chemistry-climate model. The experiments have been designed to specifically quantify the contributions from natural as well as anthropogenic factors, such as solar variability (Solar), sea surface temperatures (SSTs), the Quasi-Biennial Oscillation (QBO), stratospheric aerosols (Aerosol), greenhouse gases (GHGs), as well as the dependence on the vertical resolution in the model. The results show that, in the TTL: a cooling in tropical SSTs leads to a weakening of tropical upwelling around the tropical tropopause and hence relative downwelling and adiabatic warming of 0.4 K decade^{-1}; an increased QBO amplitude results in a 0.5 K decade^{-1} warming; increasing aerosols in the lower stratosphere lead to a 0.4 K decade^{-1} warming; a prolonged solar minimum and increased GHGs contribute about 0.3 and 0.1 K decade^{-1} to a cooling, respectively. Two simulations with different vertical resolution show that the vertical resolution can strongly influence the response of the TTL temperature to changes such as SSTs. With higher vertical resolution, an extra 0.8 K decade^{-1} warming can be simulated through the last decade, compared with results from the "standard" low vertical resolution simulation. Considering all the factors mentioned above, we compute a net 1.7 K decade^{-1} warming, which is in good agreement with the observed 1.0 K decade^{-1} warming over the past decade in the TTL. The model results indicate that the recent warming in the TTL is mainly due to internal variability, i.e. the QBO and tropical SSTs.

1 Introduction

The TTL is the transition layer from the upper troposphere to the lower stratosphere in the tropics, within which the air has distinct properties of both the troposphere and the stratosphere. The vertical range of the TTL depends on how it is defined, i.e., it can be a shallower

layer between 14–18.5 km (Fueglistaler et al., 2009) or a deeper layer of about 12–19 km (Gettelman and Forster, 2002; SPARC-CCMVal, 2010, chapter 7). As a key region for the stratosphere-troposphere coupling, the TTL acts like a "gate" for air entering into the stratosphere from the tropical troposphere. The temperature in the TTL is determined by the combined influences of latent heat release, thermally as well as dynamically driven vertical motion, and radiative cooling (Gettelman and Forster, 2002; Fueglistaler et al., 2009; Grise and Thompson, 2013). The thermal structure, static stability and zonal winds in the TTL affect the two-way interaction between the troposphere and the stratosphere (Flury et al., 2013; Simpson et al., 2009) as well as the surface climate, since the relative minimum temperature (usually known as the cold point tropopause, CPT) subsequently influences the radiation and water vapor budget (Andrews, 2010). The TTL reacts particularly sensitively to anthropogenically induced radiative, chemical and dynamical forcings of the climate system, and hence is a useful indicator for climate change (Fueglistaler et al., 2009).

Over the past decade, a remarkable warming has been captured by Global Positioning System Radio Occultation (GPS-RO) data in the TTL region (Schmidt et al., 2010; Wang et al., 2013). This might indicate a climate change signal, with possible important impacts on stratospheric climate, e.g., the tropical tropopause temperature dominates the water vapor entering the stratosphere (Dessler et al., 2013; Solomon et al., 2010; Gettelman et al., 2009; Randel and Jensen, 2013). This recent warming of the TTL is different to previous reported temperature evolutions over the last decades. So far a long-term cooling has been reported from the 1970s to 2000, although there are large differences between different datasets (Wang et al., 2012). The recent warming is therefore of great interest to study the exact reason for this warming in the TTL which might indicate a climate shift. An interesting question is also whether this warming will continue or change in sign in the future, and how well climate models can reproduce such a strong warming over one decade or longer time periods.

Based on model simulations, Wang et al. (2013) suggested that the warming around the tropical tropopause could be a result of a weaker tropical upwelling, which implies a weakening of the Brewer–Dobson circulation (BDC). However, the strengthening or weakening

of the BDC is still under debate (Butchart, 2014, and references therein). Results from observations indicate that the BDC may have slightly decelerated (Engel et al., 2009; Stiller et al., 2012), while estimates from a number of Chemistry-Climate Models (CCMs) show in contrast a strengthening of the BDC (Butchart et al., 2010; Li et al., 2008; Butchart, 2014). The reason of the discrepancy between observed and modeled BDC changes, as well as the mechanism of the BDC in response to climate change, is still under discussion (Oberländer et al., 2013; Shepherd and McLandress, 2011). The trends in the BDC may be different in different branches of the BDC (Lin and Fu, 2013; Oberländer et al., 2013). Bunzel and Schmidt (2013) show that the model configuration, i.e. the vertical resolution and the vertical extent of the model, can also impact trends in the BDC.

There are a number of other natural and anthropogenic factors besides the BDC, which influence the radiative, chemical and dynamical processes in the TTL. One prominent candidate for natural variability is the sun, which provides the energy source for the climate system. The 11 year solar cycle is the most prominent natural variation on the decadal time scale (Gray et al., 2010). Solar variability influences the temperature through direct radiative effects and indirectly through radiative effects on ozone as well as indirect dynamical effects. The maximum response in temperature occurs in the equatorial upper stratosphere during solar maximum conditions, and a distinct secondary temperature maximum can be found in the equatorial lower stratosphere around 100 hPa (SPARC-CCMVal, 2010; Gray et al., 2010). SSTs also influence the TTL by affecting the dynamical conditions and subsequently the propagation of planetary waves and hence the circulation. Increasing tropical SSTs can enhance the BDC, which in turn cools the tropical lower stratosphere through enhanced upwelling (Grise and Thompson, 2012, 2013; Oberländer et al., 2013). The QBO is the dominant mode of variability throughout the equatorial stratosphere, and has important impacts on the temperature structure as well as the distribution of chemical constituents like water vapor, methane and ozone (Baldwin et al., 2001). Stratospheric aerosols absorb outgoing long-wave radiation and lead to additional heating in the lower stratosphere, which is maximized around 20 km (Solomon et al., 2011; SPARC-CCMVal, 2010, chapter 8).

While GHGs warm the troposphere, they cool the stratosphere at the same time by releasing more radiation into space. Warming of the troposphere and cooling of the stratosphere affect the temperature in the TTL directly, and also indirectly, by changing chemical trace gas distributions and wave activities (SPARC-CCMVal, 2010).

In climate models, a sufficient high vertical resolution is important in order for models to correctly represent dynamical process, such as wave propagation into the stratosphere and wave-mean flow interactions. It is a prominent factor for a climate model to generate a self-consistent QBO (Richter et al., 2014). Meanwhile, vertical resolution is essential for a proper representation of the thermal structure in the model, e.g. models with coarse vertical resolution can not simulate the tropopause inversion layer (TIL, a narrow band of temperature inversion above the tropopause associated with a region of enhanced static stability) well (Wang et al., 2013; SPARC-CCMVal, 2010, chapter 7). Coarse vertical resolution is also still a problem for analysing the effects of El-Niño Southern Oscillation (ENSO) and the QBO onto the tropical tropopause (Zhou et al., 2001; SPARC-CCMVal, 2010, chapter 7).

In this study we use a series of simulations with NCAR's Community Earth System Model (CESM) model (Marsh et al., 2013), to quantify the contributions of the above discussed factors – Solar, SSTs, QBO, Aerosol and GHGs – to the recently observed variability in the TTL.

The details of the observed data, the model and numerical experiments, as well as a description of our methods are given in Sect. 2. The observed temperature variability in the TTL and the contributions of various factors to the recent TTL variability are addressed in Sect. 3. Section 4 focuses on the importance of the vertical resolution in one climate model. A summary and discussion are presented in Sect. 5.

2 Model simulations and method description

2.1 Fully-coupled CESM-WACCM simulations

The model used here is NCAR's Community Earth System Model (CESM), version 1.0. CESM is a fully coupled model system, including an interactive ocean (POP2), land (CLM4), sea ice (CICE) and atmosphere (CAM/WACCM) component (Marsh et al., 2013). As the atmospheric component we use the Whole Atmosphere Community Climate Model (WACCM), version 4. WACCM4 is a chemistry–climate model (CCM), with detailed middle atmospheric chemistry and a finite volume dynamical core, extending from the surface to about 140 km (Marsh et al., 2013). The standard version has 66 (W_L66) vertical levels, which means about 1 km vertical resolution in the TTL and in the lower stratosphere. All simulations use a horizontal resolution of $1.9^\circ \times 2.5^\circ$ (latitude $\times$ longitude) for the atmosphere and approximately 1 degree for the ocean.

Table 1 gives an overview of all coupled CESM simulations. A control run was performed from 1955 to 2099 (Natural run hereafter), with all natural forcings including spectrally resolved solar variability (Lean et al., 2005), a fully coupled ocean, volcanic aerosols following the SPARC CCMVal REF-B2 scenario recommendations (see details in SPARC-CCMVal, 2010) and a nudged QBO. The QBO is nudged by relaxing the modeled tropical winds to observations between 22° S and N, using a Gaussian weighting function with a half width of 10° decaying latitudinally from the equator. Full vertical relaxation extends from 86 to 64 hPa, which is half the strength of the level below and above this range and zero for all other levels (see details in Matthes et al., 2010; Hansen et al., 2013). The QBO forcing time series in CESM is determined from the observed climatology of 1953-2004 via filtered spectral decomposition of that climatology. This gives a set of Fourier coefficients that can be expanded for any day and year in the past and the future. Anthropogenic forcings like GHGs and ozone depleting substances (ODSs) are set to constant 1960s conditions. Using the Natural run as a reference, a series of four sensitivity experiments were performed by systematically switching on or off several factors. The SolarMean run uses constant solar cycle

values averaged over the past 4 observed solar cycles; the FixedSST run uses monthly varying climatological SSTs calculated from the Natural run, and therefore neglects variability from varying SSTs such as ENSO; in the NOQBO run the QBO nudging has been switched off which means weak zonal mean easterly winds develop in the tropical stratosphere. An additional simulation RCP85, uses the same forcings as the Natural run, but in addition includes increases in anthropogenic GHGs and ODSs forcings. These forcings are based on observations from 1955 to 2005, after which they follow the Representative Concentration Pathways (RCPs) RCP8.5 scenario (Meinshausen et al., 2011).

2.2 WACCM atmospheric stand-alone simulations

Instead of using the fully coupled CESM-WACCM version, WACCM can be integrated in an atmospheric stand-alone configuration, with prescribed SSTs and sea ice. Beside the standard version with 66 vertical levels (W_L66), we have also performed simulations with a finer vertical resolution, with 103 vertical levels and about 300 m vertical resolution in the TTL and lower stratosphere (W_L103) (Gettelman and Birner, 2007; Wang et al., 2013).

With the stand-alone atmospheric version an ensemble of three experiments was performed over the recent decade 2001–2010 with both WACCM versions (W_L66, W_L103) (see Table 2). Observed SSTs and spectrally resolved solar fluxes were used to produce the most realistic simulations of atmospheric variability over the past decade (2001–2010). The QBO is nudged using the same method as in the fully-coupled runs discussed above. GHGs and ODSs are based on observations for the first 5 years (2001–2005) and then follow the IPCC RCP4.5 scenario for the next 5 years (2005–2010), since no observed data were available when the simulations were started. Atmospheric aerosols were relatively constant between 2001 and 2010 since no strong volcanic eruptions occurred, and are the same as in the CESM-WACCM runs described above. All the forcings considered in this study are available from the CESM model input data repository (https://svn-ccsm-inputdata.cgd.ucar.edu/trunk/inputdata/). An additional run (W_Aerosol) was performed using the W_L103 version with observed, more realistic stratospheric aerosol forcings from the Chemistry-Climate Model Initiative (CCMI, http://www.met.reading.ac.uk/ccmi/) project.

2.3 Linear trend calculation

A standard least square regression is used to calculate the linear trend. For example, using time (t) as a single predictor, the predicted temperature (T) can be expressed as:

$$T_{\text{est}} = a + bt, \tag{1}$$

where the subscript "est" indicates that this is an estimate of T, and "b" represents the linear trend. The residuals are defined by the differences between the actual and the estimated temperature

$$e = T - T_{\text{est}}. \tag{2}$$

The "best-fit" is defined by the line that minimizes the sum of the squares of the residuals. The seasonal cycle was removed from the temperature time series before doing the regression.

The standard error (SE) is used to estimate the uncertainty of the estimated trend, which is defined by:

$$(\text{SE})^2 = \left[\sum e^2\right] / ((n-2)\left[\sum \left((t-\bar{t})^2\right)\right]), \tag{3}$$

where n is the sample size, and $\bar{t}$ is the mean value. The smaller this standard error is, the more certain is the trend.

The formula given above is, however, only correct if the individual data points are statistically independent. Considering the effect of autocorrelation, the sample size n will be reduced and an "effective sample size" can be determined by:

$$n_{\text{eff}} = n(1-r)/(1+r), \tag{4}$$

where r is the lag-1 autocorrelation coefficient.

If the trend is larger than two times the standard error, the linear regression is statistically significant at the 95 % confidence level. A brief description of the least square regression, the uncertainty of the trend, as well as the significance testing can be found in Wigley (2006).

2.4 Composite method

To estimate the contribution of the different factors to the observed temperature variability in the TTL, the composite for each factor is computed following three steps: (1) calculation of the linear trend for the respective factor over the past decade (2001–2011) from the observed, deseasonalized time series, (2) selection of time periods in the reference run, which are similar to the observed trends for the respective factor (the method of selection and the number of similar time periods depends on the factor, see below), and (3) calculation of the composite trend in temperature from all selected time periods by multiple linear regression.

With multiple (np) selected periods, the least square regression can be expressed as:

$$T_{\text{est}} = a + bt + c_1 t_1 + \cdots + c_{\text{np}} t_{\text{np}}, \tag{5}$$

where t is the time in all selected periods and b represents the composite trend, $c_1 \ldots c_{\text{np}}$ are used to estimate the "jumps" between different periods, $t_1 \ldots t_{\text{np}}$ are set to 1 for selected periods $1 \ldots np$, and equal to 0 for other periods.

As described above, the "effective sample size" (n_{eff}) is determined by the total sample size n and the autocorrelation coefficient r. The standard errors (SE) can be estimated from equation (3) with the degrees of freedom $n_{\text{eff}} - np - 2$. For the estimated trend b, the test statistics

$$t\_test = b/SE, \tag{6}$$

has the Student's t-distribution with $n_{\text{eff}} - np - 2$ degrees of freedom.

The composite trend is then calculated for each of the two runs (e.g. Natural and SolarMean) to be compared as well as for their differences. Both runs have the same configuration and forcings, except for the long-term variability of the respective factor (e.g. Solar). The contribution of this factor is then quantified by the trend differences between the two runs.

Special attention is given to the region 20° S–20° N latitude and 16–20 km height, which is mainly the observed warming area in the TTL (see below). Hereafter, we use the average trend over this area to discuss the exact contribution of every factor to the temperature trend in the TTL.

2.5 Forcings in observations and model simulations

Figure 1 shows the time series of both natural and anthropogenic forcings over past and future decades in the observations (black) and in the Natural model experiment (blue). Periods with a similar trend as the recent decade (2001–2011) are shown with straight lines.

Observations of the solar variability show that the total solar irradiance (TSI) exhibits a clear 11 year solar cycle (SC) variation of about 1 W m^{-2} between sunspot minimum (S_{min}) and sunspot maximum (S_{max}) in the past (Gray et al., 2010), with a delayed and smaller amplitude return to maximum conditions in the recent decade (Fig. 1a). The future projection is a repetition of the last four observed solar cycles. Similar periods of decreasing TSI can be found in the periods 1958–1968, 2001–2011, 2045–2055, and 2089–2099. A composite trend is then constructed by applying multiple linear regression to all four selected periods in the Natural as well as the SolarMean experiments (Eq. 5). By comparing the trends in these two runs with and without solar cycle variations, the effect of solar variability on the temperature trend in the TTL can be estimated.

Figure 1b shows the variability of tropical (20° S–20° N) SSTs for the last five decades from observations (Hadley Center Updates and supplementary information available from http://www.metoffice.gov.uk/hadobs/hadisst, black lines) and up to 2099 from the Natural coupled CESM-WACCM model experiment (blue line). Both the observed and simulated tropical SSTs show a statistically significant (over 95 %) decrease from 2001 to 2011. A similar decrease in tropical SSTs can be found during the periods 1956–1968, 1980–1991, 2001–2014, 2028–2043 and 2047–2057. Periods longer than 10 years have been selected from the filtered tropical SST time series. Filtering has been performed twice with

a Butterworth low-pass filter (longer than 30 years). Note that there is also a strong drop in SSTs around 1992 in the model, which does not occur in the observations. This might be caused by an overestimated response to the Pinatubo eruption in CESM-WACCM (Marsh et al., 2013; Meehl et al., 2012). By comparing the Natural run, where SSTs are calculated explicitly, and the FixedSST run where SSTs are climatologically prescribed, the effect of interactively calculated SSTs can be determined.

Instead of a decrease in tropical SSTs, the QBO amplitude shows an increase during the selected two periods (Fig. 1c). The observed QBO amplitude has been calculated from the absolute values of deseasonalized monthly mean anomalies of the zonal mean zonal wind at 70 hPa (from the FU Berlin: http://www.geo.fu-berlin.de/en/met/ag/strat/produkte/qbo/index.html); in our model simulations it is computed where the QBO has been nudged. The time periods of increasing QBO amplitude are selected by the same as the procedure as for the tropical SSTs. By comparing the Natural and the NOQBO experiments, the effect of a (nudged) QBO on the temperature trends in the TTL can be estimated.

As shown in Fig. 1d, GHGs show a steady increase after 2001. The increasing rate of global CO_2 release from 2001 to 2011 is close to the RCP8.5 scenario, which we used in our RCP85 run. By comparing the experiments with (RCP85) and without (Natural) GHG increases, the GHG effect on the observed temperature trend can be estimated. To avoid possible uncertainties due to the short time series, a longer time period from 2001 through 2050 will be used to compare the Natural and the RCP85 run.

Similar to the GHGs, observed stratospheric aerosols (aerosol optical depth (AOD)) have been steadily increasing since 2001 (Solomon et al., 2011) in the lower stratosphere (18–32 km) (Fig. 1e). This increase in stratospheric aerosol loading is attributed to a number of small volcanic eruptions and anthropogenically released aerosols transported into the stratosphere during the Asian Monsoon (Bourassa et al., 2012; Neely et al., 2013). An aerosol data set has been constructed for the CCMI project (ftp://iacftp.ethz.ch/pub_read/luo/ccmi/) and is similar to the data described by Solomon et al. (2011). The comparison of the two experiments with different AOD data sets will shed light on the stratospheric aerosol contribution to the observed temperature trend.

All natural and anthropogenic forcings will be discussed with respect to their contribution to the temperature variability in TTL in the following section.

3 Quantification of observed temperature variability

3.1 Observed temperature variability in the TTL

Figure 2 shows the latitude-height section of the linear temperature trend for the period 2001–2011 estimated from GPS-RO observations (see details of the GPS-RO data in Wang et al., 2013). A remarkable and statistically significant warming occurs around the TTL between about 20° south to north and from 15 to 20 km height. The warming in the TTL is 1.0 K decade^{-1} on average, with a maximum of about 1.8 K decade^{-1} directly at the tropical tropopause around 17 to 18 km. This figure is an extension of earlier work by Schmidt et al. (2010) and Wang et al. (2013) and shows an unexpected warming, despite the steady increase in GHGs which imply a cooling of this region. Therefore it is interesting to study whether this warming is simply a phenomenon of the past decade and the result of internal atmospheric variability, or whether it will persist for longer and therefore modify trace gas transport from the troposphere into the stratosphere.

Please note that this decadal warming in the TTL may vary in magnitude if different end years are selected due to the relative short length of the time series. The warming is weaker if end years of 2012 or 2013 are chosen (seed also Figs. S1 and S2). In the following investigations, we keep the period from 2001 through 2011 to be most consistent with our WACCM simulations (2001–2010). We will explain the temperature variability within a time period of about one decade. This decadal variability may change sign from decade to decade if it is mainly caused by natural/internal variability. However, it is still very important to understand the reasons and mechanisms behind these internal variability modes as it might eventually enhance our decadal to multi-decadal predictive skills.

3.2 Contribution of solar variability

Figures 3a and b show the composite temperature trends for periods with decreasing solar irradiance (1958–1968, 2001–2011, 2045–2055, and 2089–2099) for the Natural and SolarMean runs, respectively. The Natural run shows a partially significant temperature increase from S_{max} to S_{min} of about 0.1 K decade^{-1} on average around the TTL, while the SolarMean run shows on average a partially statistically significant temperature increase of 0.4 K decade^{-1} in the tropics and subtropics. Figure 3c shows the differences in temperature trends between the Natural and the SolarMean experiments. Solar variability thus contributed to a cooling of about 0.3 K decade^{-1} in the TTL during periods with similar solar variability to the recent decade.

3.3 Contribution of tropical SSTs

Figure 4 shows the composite temperature trends for the periods with decreasing tropical SSTs (1956–1968, 1980–1991, 2001–2014, 2028–2043 and 2047–2057) for both the Natural and the FixedSST runs (Fig. 4a and b), as well as their differences (Fig. 4c). While the Natural experiment shows a partially statistically significant temperature increase of 0.4 K decade^{-1} on average (1.0 K decade^{-1} in maximum) in the TTL, the FixedSST experiment shows an insignificant (0–0.2 K decade^{-1}) temperature change during periods with similar SST variability to the recent decade. A decrease in tropical SSTs contributes therefore to a statistically significant warming of 0.4 K decade^{-1} on average (0.6 K decade^{-1} in maximum) in the TTL (Fig. 4c).

3.4 Contribution of the QBO

Figures 5a and b show composite temperature trends, for periods with increasing QBO amplitudes (2003–2017 and 2054–2068) for the Natural and the NOQBO experiment, respectively. While the Natural experiment shows an insignificant warming of 0.3 K decade^{-1} on average (0.8 K decade^{-1} in maximum) in the TTL, the NOQBO run shows a slight but statistically significant cooling for the same period. The differences in Fig. 5c indicate that

the increased QBO amplitude contributes to a warming of 0.5 K decade^{-1} on average (0.8 K decade^{-1} in maximum) in the TTL. Another effect of the QBO is the statistically significant cooling trend seen in the tropical middle stratosphere above 22 km in the Natural run. This QBO effect may help to explain the observed tropical cooling (see Fig. 2). Please note, however, that, CESM1.0 used for these simulations, cannot generate a self-consistent QBO and hence uses wind nudging, which might cause problems when estimating QBO effects on temperature variability in the tropical lower stratosphere (Marsh et al., 2013; Morgenstern et al., 2010).

3.5 Contribution of GHGs

The temperature trends from both the Natural and the RCP85 experiments between 2001 and 2050 are shown in Figs. 6a and b, respectively. As expected, increasing GHGs in the RCP85 experiment tend to cool the lower and warm the upper troposphere, with a zero line slightly above the tropopause. Hence the effect of global warming is seen in Fig. 6c with a weak averaged cooling trend in the TTL of about 0.1 K decade^{-1}. Further estimates were also calculated with different ending years for both the Natural and the RCP85 runs (not shown). The longer the chosen time period the clearer the patterns related to the GHG effect, i.e. a clear warming in the upper troposphere and a cooling in the lower stratosphere with the zero-line just above the tropopause.

3.6 Contribution of stratospheric aerosols

The temperature trends from the simulations with relative constant AOD values (W_L103) and with more realistic CCMI aerosols (W_Aerosol) are shown in Figs. 7a and b, respectively. A clearly stronger and more statistically significant warming pattern can be seen around the tropical tropopause in the W_Aerosol run as compared to the W_L103 run. The effect of increasing stratospheric aerosols is estimated to be 0.4 K decade^{-1} warming in the TTL (Fig. 7c). Please note that there may exist uncertainties for this result since we have only 10 years of simulations for the W_Aerosol run. With such a short time period, and after

considering autocorrelation effects, the "effective sample size" will be strongly reduced and hence will cause all strong trends to be insignificant. The trends in the W_L103 run in contrast have been estimated by the ensemble mean of the three simulations and might not suffer from this problem.

To confirm the contributions of different factors from the composite analysis described above, a linear regression is additionally performed to estimate the contributions of Solar, SST, QBO and GHGs to the TTL temperature variability over the whole time series 1955–2099, from the Natural, SolarMean, FixSST, NOQBO and RCP85 runs. The time series of TTL temperature differences (comparative run minus control run, e.g., RCP85 - Natural), is regressed onto the specific factor (e.g. GHGs) to investigate the impacts of this factor on the TTL temperature variability. The results are consistent with the composite method presented in Figs. 3–7, which show positive temperature anomalies due to decreasing SSTs and increasing QBO amplitude, and negative temperature anomalies due to decreasing solar radiation and increasing GHGs in the TTL. The estimated contributions of Solar, SST, QBO and GHGs from the linear regression are, however, weaker than those from the composite method. The composite method is therefore a composite of "strong events", with remarkable decadal trend in these factors, and is thus useful to explain the recent decadal warming in the TTL.

4 Effects of the vertical resolution

To estimate not only anthropogenic and natural contributions to the recent TTL temperature variability but also the effects of the vertical resolution in the model, Figs. 8a and b show the temperature trends in the standard W_L66 run and the differences in temperature trends between the high-resolution (W_L103) and the standard (W_L66) runs, respectively. The W_L103 run (Fig. 8b) shows a statistically significant 0.6 K decade^{-1} warming on average over the past decade around the TTL, which maximizes at 1.2 K decade^{-1}. The trends in

the W_L103 simulation in this paragraph were estimated by the linear regression method introduced in section 2.4, which is then applied to the three simulations of the W_L103 run. The resulting trends are almost the same as in Fig. 7b, but the significances are quite different because there are more sample sizes for the significance test. The standard W_L66 run (Fig. 8a) does not capture the warming. The only difference between the two experiments is the vertical resolution, meaning that a higher vertical resolution captures the warming in the TTL better than the standard vertical resolution, reaching up to $0.8\,\mathrm{K\,decade^{-1}}$ (Fig. 8b). Wang et al. (2013) showed that the tropical upwelling in the lower stratosphere has weakened over the past decade in the W_L103 run, while there is no significant upwelling trend in the standard vertical resolution (W_L66) run. The decreasing tropical upwelling in the W_L103 run might be the reason for the extra warming in the TTL compared to the W_L66 run, since dynamical changes would lead to adiabatic warming. More detailed investigation will be given in the following section.

4.1 Changes in the Brewer–Dobson circulation

To investigate dynamical differences between the two experiments with standard and higher vertical resolution in more detail, the Transformed Eulerian Mean (TEM) diagnostics (Andrews et al., 1987) was applied to investigate differences in the wave propagation and Brewer–Dobson circulation (BDC) in the climatological mean as well as in the decadal trend.

Figure 9 shows the annual mean climatology of the BDC (arrows for the meridional and vertical wind components), the zonal mean zonal wind (blue contour lines) and the temperature (filled colours) from the W_L103 run (Fig. 9a), as well as the differences between the W_L103 and the W_L66 runs (Fig. 9c). The BDC shows an upwelling in the tropics and a downwelling through mid to high latitudes in the annual mean. With finer vertical resolution (W_L103) the model produces a stronger upwelling in the tropics (and a consistent cooling) up to the tropopause region, with westerly wind anomalies above. This strengthened tropical upwelling can not continue further up because of the westerly wind anomalies blocking transport into the subtropics and finally diminishing. Above the tropical tropopause there is

less upwelling and in particular more transport from the subtropics into the tropical TTL, leading to a stronger warming around 19 km in the W_L103 experiment. These changes in the BDC indicate a strengthening of its lower branch, and a weakening of the transition branch (Lin and Fu, 2013). This is consistent with previous work by Bunzel and Schmidt (2013), which indicates a weaker upward mass flux around 70 hPa in a model experiment with higher vertical resolution.

The annual mean trends in the W_L103 experiment indicate a further strengthening of the BDC lower branch over the past decade in this simulation (Fig. 9b) and a statistically significant weakening of the transition branch resulting in significant warming of 1 to 2 K decade^{-1} in the TTL. In particular the trends in the TTL are stronger in the W_L103 compared to the W_L66 experiment (Fig. 9d). This is consistent with previous work by Bunzel and Schmidt (2013), which shows also stronger changes in the BDC using a model with higher vertical resolution.

In summary, the finer vertical resolution can enhance the upward wave propagation from the tropics. This enhanced wave propagation speeds up the lower branch of the BDC in the upper troposphere and slows down the transition branch of the BDC. These changes in the BDC and corresponding wave-mean flow interactions (not shown) finally result in the statistically significant warming in the TTL.

Bunzel and Schmidt (2013) attributed the differences in the BDC to different vertical resolutions which tend to reduce the numerical diffusion through the tropopause and the secondary meridional circulation. Our results show that the strong warming and subsequent enhanced static stability (not shown) above the tropopause may also influence wave dissipation and propagation around the tropopause. Oberländer et al. (2013) point out that an increase of tropical SSTs enhances the BDC. This is consistent with our results, which show a weakening of the BDC in the lower stratosphere following a decrease in tropical SSTs. At the same time, this response of the stratosphere to the surface can be better represented by a model with finer vertical resolution.

5 Summary and discussion

Based on a series of sensitivity simulations with NCAR's CESM-WACCM model, the contribution of different natural (solar, QBO, tropical SSTs) and anthropogenic (GHGs, ODS) factors to the observed warming of the TTL over the past decade from 2001 through 2011 has been studied. By comparing model experiments with and without the respective factors and combining a number of periods with similar trends in a composite, the contribution of each factor has been quantified in order to explain the causes of the observed recent decadal variability in GPS-RO data.

A decrease in tropical SSTs, an increase in stratospheric aerosol loading and an increase in the QBO amplitude contribute each about 0.4, 0.4 and 0.5 K decade^{-1} to this warming, respectively, resulting in a total 1.3 K decade^{-1} warming, while the delay and smaller amplitude of the current solar maximum and the steady increase in GHGs and ODS concentrations contribute each about 0.3 and 0.1 K decade^{-1} to a cooling, respectively, resulting in a total 0.4 K decade^{-1} cooling. The vertical resolution of the model strongly influences the TTL response to the surface mainly via dynamical changes, i.e. an enhancement of the lower branch of the BDC and a decrease of the transition (upper) branch in response to the decreasing tropical SSTs. This leads to a 0.8 K decade^{-1} extra warming in the TTL in the finer vertical resolution experiment as compared to the standard vertical resolution. Adding all natural and anthropogenic factors, as well as the contribution from finer vertical resolution, we estimate a total modeled warming of 1.7 K decade^{-1} around the TTL (Table 3), which is higher than the observed 1.0 K decade^{-1} warming from GPS-RO data. The estimate from the model is higher because we estimated the total contribution from all factors and assumed that all factors are independent from each other and therefore the individual contributions can be linearly added. However, in reality non-linear interactions between the different factors occur which we did not take into account in our first order linear approach. This uncertainty from the non-linear interactions can be estimated by our W_Aerosol run. The W_Aerosol run, with almost all observed forcings considered in this study, can be seen as the most realistic simulation. The TTL warming in the W_Aerosol

run is 1.0 K decade^{-1} on average and 1.6 K decade^{-1} in maximum (Fig. 7b), which are very close to the observed trend. This in turn indicates, that missing non-linear interactions, can overestimate the warming up to 0.7 K decade^{-1} compared to the observed 1.0 K decade^{-1} warming.

According to our experiments, one of the primary factors contributing to the recent warming in the TTL is the natural variability in tropical SSTs. However, the mechanism of the TTL response to SSTs awaits further investigation. One key issue is how much improvement we can expect from using a fully-coupled ocean-atmosphere model instead of atmosphere only model with prescribed SSTs. Our W_L66 and W_L103 simulations indicate that the atmosphere-only model may not correctly reproduce the response of TTL variability to SST, but can be improved with finer vertical resolution.

Another important factor in contributing to the recent warming in the TTL is the QBO amplitude. The QBO amplitude is closely related to the tropical upwelling Kawatani and Hamilton (2013). A regression of temperature differences onto the differences in the vertical component of BDC between the Natural and NOQBO run, shows a very similar result than the regression of temperature onto the QBO time series (not shown). The QBO may influence the TTL temperature by modifying the BDC.

Fig. S3 clearly shows decadal to multidecadal fluctuations in temperature in the TTL from both, the Modern Era Retrospective-analysis for Research and Applications (MERRA) reanalysis data, and our Natural and RCP85 runs, which provide a strong support to the internal variability dominated TTL warming over past decade.

The external forcings (solar, GHGs, ODS) contribute relatively little to the temperature variability in the TTL, except for the stratospheric aerosols. Internal variability, i.e. the QBO and tropical SSTs, seem to be mainly responsible for the recent TTL warming.

Acknowledgements. W. Wang is supported by a fellowship of the China Scholarship Council (CSC) at FU Berlin. This work was also performed within the Helmholtz-University Young Investigators Group NATHAN, funded by the Helmholtz-Association through the president's Initiative and Networking Fund, and the GEOMAR – Helmholtz-Zentrum für Ozeanforschung in Kiel. The model calculations have been performed at the Deutsche Klimarechenzentrum (DKRZ) in Hamburg, Germany.

We thank F. Hansen, C. Petrick, R. Thiéblemont and S. Wahl for carrying out some of the simulations. We appreciate discussion about the statistical methods with D. Maraun and the help with grammar checking of L. Neef .

The service charges for this open access publication have been covered by a Research Centre of the Helmholtz Association.

References

Andrews, D. G.: An Introduction to Atmospheric Physics, Cambridge University Press, New York, 2010.

Andrews, D. G., Holton, J. R., and Leovy, C. B.: Middle Atmosphere Dynamics, vol. 40, Academic Press, San Diego, 1987.

Baldwin, M. P., Gray, L. J., Dunkerton, T. J., Hamilton, K., Haynes, P. H., Randel, W. J., Holton, J. R., Alexander, M. J., Hirota, I., Horinouchi, T., Jones, D. B. A., Kinnersley, J. S., Marquardt, C., Sato, K., and Takahashi, M.: The quasi-biennial oscillation, Rev. Geophys., 39, 179–229, doi:10.1029/1999RG000073, 2001.

Balmaseda, M. A., Trenberth, K. E., and Källén, E.: Distinctive climate signals in reanalysis of global ocean heat content, Geophys. Res. Lett., 40, 1754–1759, doi:10.1002/grl.50382, 2013.

Bourassa, A. E., Robock, A., Randel, W. J., Deshler, T., Rieger, L. A., Lloyd, N. D., Llewellyn, E. T., and Degenstein, D. A.: Large volcanic aerosol load in the stratosphere linked to Asian monsoon transport, Science, 337, 78–81, doi:10.1126/science.1219371, 2012.

Bunzel, F. and Schmidt, H.: The Brewer–Dobson circulation in a changing climate: impact of the model configuration, J. Atmos. Sci., 70, 1437–1455, doi:10.1175/JAS-D-12-0215.1, 2013.

Butchart, N.: The Brewer–Dobson circulation, Rev. Geophys., 52, 157–184, doi:10.1002/2013RG000448, 2014.

Butchart, N., Cionni, I., Eyring, V., Shepherd, T. G., Waugh, D. W., Akiyoshi, H., Austin, J., Bruhl, C., Chipperfield, M. P., Cordero, E., Dameris, M., Deckert, R., Dhomse, S., Frith, S. M., Garcia, R. R., Gettelman, A., Giorgetta, M. A., Kinnison, D. E., Li, F., Mancini, E., McLandress, C., Pawson, S., Pitari, G., Plummer, D. A., Rozanov, E., Sassi, F., Scinocca, J. F., Shibata, K., and Tian, W.: Chemistry-climate model simulations of twenty-first century stratospheric climate and circulation changes, J. Climate, 23, 5349–5374, doi:10.1175/2010JCLI3404.1, 2010.

Dessler, A. E., Schoeberl, M. R., Wang, T., Davis, S. M., and Rosenlof, K. H.: Stratospheric water vapor feedback., P. Natl. Acad. Sci. USA, 110, 18087–18091, doi:10.1073/pnas.1310344110, 2013.

Engel, A., Mobius, T., Bonisch, H., Schmidt, U., Heinz, R., Levin, I., Atlas, E., Aoki, S., Nakazawa, T., Sugawara, S., Moore, F., Hurst, D., Elkins, J., Schauffler, S., Andrews, A., and Boering, K.: Age of stratospheric air unchanged within uncertainties over the past 30 years, Nat. Geosci., 2, 28–31, doi:10.1038/ngeo388, 2009.

England, M. H., McGregor, S., Spence, P., Meehl, G. A., Timmermann, A., Cai, W., Gupta, A. S., McPhaden, M. J., Purich, A., and Santoso, A.: Recent intensification of wind-driven circulation in the Pacific and the ongoing warming hiatus, Nature Climate Change, 4, 222–227, doi:10.1038/nclimate2106, 2014.

Flury, T., Wu, D. L., and Read, W. G.: Variability in the speed of the Brewer–Dobson circulation as observed by Aura/MLS, Atmos. Chem. Phys., 13, 4563–4575, doi:10.5194/acp-13-4563-2013, 2013.

Fueglistaler, S., Dessler, A., Dunkerton, T., Folkins, I., Fu, Q., and Mote, P. W.: Tropical tropopause layer, Rev. Geophys., 47, 1004, doi:10.1029/2008RG000267, 2009.

Fyfe, J. C. and Gillett, N. P.: Recent observed and simulated warming, Nature Clim. Change, 4, 150–151, doi:10.1038/nclimate2111, 2014.

Fyfe, J. C., Gillett, N. P., and Zwiers, F. W.: Overestimated global warming over the past 20 years, Nature Climate Change, 3, 767–769, doi:10.1038/nclimate1972, 2013.

Gettelman, A. and Birner, T.: Insights into tropical tropopause layer processes using global models, J. Geophys. Res., 112, D23104, doi:10.1029/2007JD008945, 2007.

Gettelman, A. and Forster, P. D. F.: A climatology of the tropical tropopause layer, J. Meteor. Soc. Jpn., 80, 911–924, doi:10.2151/jmsj.80.911, 2002.

Gettelman, A., Birner, T., Eyring, V., Akiyoshi, H., Bekki, S., Brühl, C., Dameris, M., Kinnison, D. E., Lefevre, F., Lott, F., Mancini, E., Pitari, G., Plummer, D. A., Rozanov, E., Shibata, K., Stenke, A., Struthers, H., and Tian, W.: The Tropical Tropopause Layer 1960–2100, Atmos. Chem. Phys., 9, 1621–1637, doi:10.5194/acp-9-1621-2009, 2009.

Gray, L. J., Beer, J., Geller, M., Haigh, J. D., Lockwood, M., Matthes, K., Cubasch, U., Fleitmann, D., Harrison, G., Hood, L., Luterbacher, J., Meehl, G. A., Shindell, D., van Geel, B., and White, W.: Solar influences on climate, Rev. Geophys., 48, RG4001, doi:10.1029/2009RG000282, 2010.

Grise, K. M. and Thompson, D. W.: Equatorial planetary waves and their signature in atmospheric variability, J. Atmos. Sci., 69, 857–874, doi:10.1175/JAS-D-11-0123.1, 2012.

Grise, K. M. and Thompson, D. W.: On the signatures of equatorial and extratropical wave forcing in tropical tropopause layer temperatures, J. Atmos. Sci., 70, 1084–1102, doi:10.1175/JAS-D-12-0163.1, 2013.

Hansen, F., Matthes, K., and Gray, L.: Sensitivity of stratospheric dynamics and chemistry to QBO nudging width in the chemistry–climate model WACCM, J. Geophys. Res., 118, 10–464, doi:10.1002/jgrd.50812, 2013.

Kawatani, Y. and Hamilton, K.: Weakened stratospheric quasibiennial oscillation driven by increased tropical mean upwelling, Nature, 497, 478–481, doi:10.1038/nature12140, 2013.

Kosaka, Y. and Xie, S.-P.: Recent global-warming hiatus tied to equatorial Pacific surface cooling, Nature, 501, 403–407, doi:10.1038/nature12534, 2013.

Lean, J., Rottman, G., Harder, J., and Kopp, G.: SORCE contributions to new understanding of global change and solar variability, Sol. Phys., 230, 27–53, doi:10.1007/s11207-005-1527-2, 2005.

Li, F., Austin, J., and Wilson, J.: The strength of the Brewer–Dobson circulation in a changing climate: coupled chemistry-climate model simulations, J. Climate, 21, 40–57, doi:10.1175/2007JCLI1663.1, 2008.

Lin, P. and Fu, Q.: Changes in various branches of the Brewer–Dobson circulation from an ensemble of chemistry climate models, J. Geophys. Res., 118, 73–84, doi:10.1029/2012JD018813, 2013.

Marsh, D. R., Mills, M. J., Kinnison, D. E., Lamarque, J.-F., Calvo, N., and Polvani, L. M.: Climate change from 1850 to 2005 simulated in CESM1 (WACCM), J. Climate, 26, 7372–7391, doi:10.1175/JCLI-D-12-00558.1, 2013.

Matthes, K., Marsh, D. R., Garcia, R. R., Kinnison, D. E., Sassi, F., and Walters, S.: Role of the QBO in modulating the influence of the 11 year solar cycle on the atmosphere using constant forcings, J. Geophys. Res., 115, 18110, doi:10.1029/2009JD013020, 2010.

Meehl, G. A., Washington, W. M., Arblaster, J. M., Hu, A., Teng, H., Tebaldi, C., Sanderson, B. N., Lamarque, J.-F., Conley, A., Strand, W. G., and White, J. B.: Climate system response to external forcings and climate change projections in CCSM4, J. Climate, 25, 3661–3683, doi:10.1175/JCLI-D-11-00240.1, 2012.

Meinshausen, M., Smith, S. J., Calvin, K., Daniel, J. S., Kainuma, M. L. T., Lamarque, J.-F., Matsumoto, K., Montzka, S., Raper, S., Riahi, K., Thomson, A., Velders, G. J. M., and van Vuuren, D. P.: The RCP greenhouse gas concentrations and their extensions from 1765 to 2300, Climatic Change, 109, 213–241, doi:10.1007/s10584-011-0156-z, 2011.

Morgenstern, O., Giorgetta, M. A., Shibata, K., Eyring, V., Waugh, D. W., Shepherd, T. G., Akiyoshi, H., Austin, J., Baumgaertner, A. J. G., Bekki, S., Braesicke, P., Brühl, C., Chipperfield, M. P., Cugnet, D., Dameris, M., Dhomse, S., Frith, S. M., Garny, H., Gettelman, A., Hardiman, S. C., Hegglin, M. I., Jöckel, P., Kinnison, D. E., Lamarque, J.-F., Mancini, E., Manzini, E., Marchand, M., Michou, M., Nakamura, T., Nielsen, J. E., Olivié, D., Pitari, G., Plummer, D. A.,

Rozanov, E., Scinocca, J. F., Smale, D., Teyssèdre, H., Toohey, M., Tian, W., and Yamashita, Y.: Review of the formulation of present-generation stratospheric chemistry-climate models and associated external forcings, J. Geophys. Res., 115, D00M02, doi:10.1029/2009JD013728, 2010.

Neely, R. R., Toon, O. B., Solomon, S., Vernier, J. P., Alvarez, C., English, J. M., Rosenlof, K. H., Mills, M. J., Bardeen, C. G., Daniel, J. S., and Thayer, J. P.: Recent anthropogenic increases in SO_2 from Asia have minimal impact on stratospheric aerosol, Geophys. Res. Lett., 40, 999–1004, doi:10.1002/grl.50263, 2013.

Oberländer, S., Langematz, U., and Meul, S.: Unraveling impact factors for future changes in the Brewer–Dobson circulation, J. Geophys. Res., 118, 10–296, doi:10.1002/jgrd.50775, 2013.

Randel, W. J. and Jensen, E. J.: Physical processes in the tropical tropopause layer and their roles in a changing climate, Nat. Geosci., 6, 169–176, doi:10.1038/ngeo1733, 2013.

Randel, W. J., Shine, K. P., Austin, J., Barnett, J., Claud, C., Gillett, N. P., Keckhut, P., Langematz, U., Lin, R., Long, C., Mears, C., Miller, A., Nash, J., Seidel, D. J., Thompson, D. W. J., Wu, F., and Yoden, S.: An update of observed stratospheric temperature trends, J. Geophys. Res., 114, D02107, doi:10.1029/2008JD010421, 2009.

Richter, J. H., Solomon, A., and Bacmeister, J. T.: On the simulation of the quasi-biennial oscillation in the Community Atmosphere Model, version 5, Journal of Geophysical Research: Atmospheres, 119, doi:10.1002/2013JD021122, 2014.

Schmidt, T., Wickert, J., and Haser, A.: Variability of the upper troposphere and lower stratosphere observed with GPS radio occultation bending angles and temperatures, Adv. Space. Res., 46, 150–161, doi:10.1016/j.asr.2010.01.021, 2010.

Shepherd, T. G. and McLandress, C.: A robust mechanism for strengthening of the Brewer–Dobson circulation in response to climate change: critical-layer control of subtropical wave breaking, J. Atmos. Sci., 68, 784–797, doi:10.1175/2010JAS3608.1, 2011.

Simpson, I. R., Blackburn, M., and Haigh, J. D.: The role of eddies in driving the tropospheric response to stratospheric heating perturbations, J. Atmos. Sci., 66, 1347–1365, doi:10.1175/2008JAS2758.1, 2009.

Solomon, S., Rosenlof, K. H., Portmann, R. W., Daniel, J. S., Davis, S. M., Sanford, T. J., and Plattner, G.-K.: Contributions of stratospheric water vapor to decadal changes in the rate of global warming, Science, 327, 1219–1223, doi:10.1126/science.1182488, 2010.

Solomon, S., Daniel, J., Neely, R., Vernier, J.-P., Dutton, E., and Thomason, L.: The persistently variable "background" stratospheric aerosol layer and global climate change, Science, 333, 866–870, doi:10.1126/science.1206027, 2011.

SPARC-CCMVal: SPARC Report on the Evaluation of Chemistry-Climate Models, SPARC Report 5, WCRP-132, WMO/TD-1526, 2010.

Stiller, G. P., von Clarmann, T., Haenel, F., Funke, B., Glatthor, N., Grabowski, U., Kellmann, S., Kiefer, M., Linden, A., Lossow, S., and López-Puertas, M.: Observed temporal evolution of global mean age of stratospheric air for the 2002 to 2010 period, Atmos. Chem. Phys., 12, 3311–3331, doi:10.5194/acp-12-3311-2012, 2012.

Wang, J. S., Seidel, D. J., and Free, M.: How well do we know recent climate trends at the tropical tropopause?, J. Geophys. Res., 117, 09 118, doi:10.1029/2012JD017444, 2012.

Wang, W., Matthes, K., Schmidt, T., and Neef, L.: Recent variability of the tropical tropopause inversion layer, Geophys. Res. Lett., 40, 6308–6313, doi:10.1002/2013GL058350, 2013.

Wigley, T.: Appendix A: Statistical issues regarding trends, in: Temperature Trends in the Lower Atmosphere: Steps for Understanding and Reconciling Differences, edited by: Karl, T. R., Hassol, S. J., Miller, C. D., and Murray, W. L., A Report by Climate Change Science Program and the Subcommittee on Global Change Research, Washington, DC, USA, UNT Digital Library, 129–139, 2006.

Zhou, X.-L., Geller, M. A., and Zhang, M.: Cooling trend of the tropical cold point tropopause temperatures and its implications, J. Geophys. Res., 106, 1511–1522, doi:10.1029/2000JD900472, 2001.

Table 1. Overview of fully-coupled CESM-WACCM simulations (1955–2099).

Simulations	Natural Forcings	GHGs
Natural	All natural forcings, including transit solar variability, fully coupled ocean, prescribed volcanic aerosols and nudged QBO	Fixed GHGs to 1960s state
SolarMean	As Natural run, but with fixed solar radiation	Fixed
FixedSST	As Natural run, but with fixed SSTs	Fixed
NOQBO	As Natural run, but without QBO nudging	Fixed
RCP85	As Natural run	RCP8.5 scenario

Table 2. Overview of WACCM atmospheric stand-alone simulations (2001–2010).

Simulations	Number of Simulations	Vertical levels	Forcings	Stratospheric aerosols
W_L103	3	103	Observed solar variability and SSTs, nudged QBO, GHGs in RCP4.5 scenario	Volcanic aerosols from CCMVal-2
W_L66	3	66	As W_L103	As W_L103
W_Aerosol	1	103	As W_L103	Stratospheric aerosols from CCMI

Table 3. Summary of contributions from the varying factors to the observed TTL warming between 2001 and 2011, in the region 20° S–20° N latitude and 16–20 km.

Factors	Solar	SSTs	QBO	GHGs	Aerosols	Vertical Resolution	**Total**
Contribution (K decade^{-1})	-0.3	0.4	0.5	-0.1	0.4	0.8	**1.7**
Observation							**1.0**

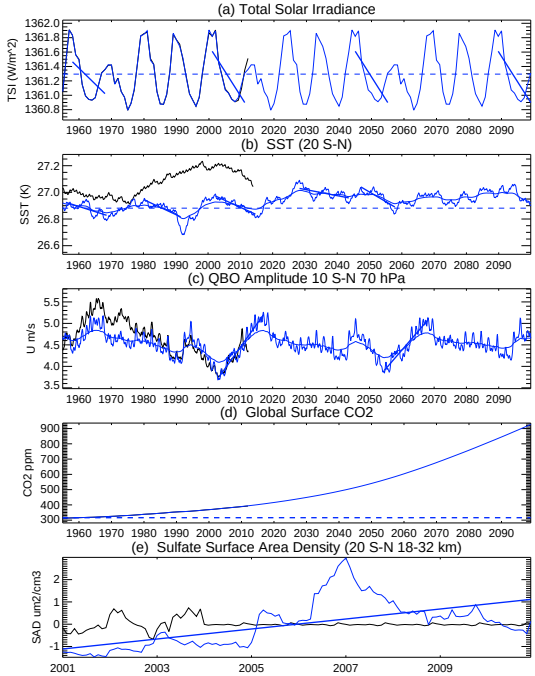
(a) Total Solar Irradiance
TSI (W/m^2)
1362.0
1361.8
1361.6
1361.4
1361.2
1361.0
1360.8
1960 1970 1980 1990 2000 2010 2020 2030 2040 2050 2060 2070 2080 2090
(b) SST (20 S-N)
SST (K)
27.2
27.0
26.8
26.6
1960 1970 1980 1990 2000 2010 2020 2030 2040 2050 2060 2070 2080 2090
(c) QBO Amplitude 10 S-N 70 hPa
U m/s
5.5
5.0
4.5
4.0
3.5
1960 1970 1980 1990 2000 2010 2020 2030 2040 2050 2060 2070 2080 2090
(d) Global Surface CO2
CO2 ppm
900
800
700
600
500
400
300
1960 1970 1980 1990 2000 2010 2020 2030 2040 2050 2060 2070 2080 2090
(e) Sulfate Surface Area Density (20 S-N 18-32 km)
SAD um2/cm3
2
1
0
-1
2001 2003 2005 2007 2009

Figure 1. Time series of forcing data sets used for the simulations from 1955 through 2099. **(a)** TSI from observations (black) until 2012, the *Natural* run (solid blue) and the *SolarMean* run (dashed blue). The last four solar cycles have been repeated into the future. **(b)** SSTs from observations HadISSTs (see details in text) (black), the *Natural* run (solid blue) and the *FixedSST* run (dashed blue). The SSTs in observations and the *Natural* run have been smoothed by a low-pass ($T > 30$ years) Butterworth Filter. The smooth blue line has been smoothed twice by the same low-pass Butterworth Filter. **(c)** Same as in **(b)**, but for the QBO amplitude calculated from zonal mean zonal winds at 70 hPa and between 10° S and 10° N. **(d)** Global surface CO_2 concentration from observations (black, overlapped with the blue line), the *RCP85* run (solid blue) and the *Natural* run (dashed blue). **(e)** AOD (532 nm, 18–32 km) from the CCMI (Solid blue) and the CCMVal2 (black) projects for the time 2001–2010. The blue solid straight lines in each subfigure are the linear fits of the respective forcing for the selected decade.

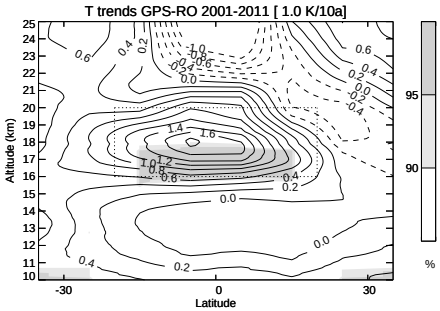

Figure 2. Latitude-height section of linear temperature trends over the past decade (2001–2011) from *GPS-RO* data over a height range from 10 to 25 km and 35° S to 35° N latitude; contour interval: 0.2 K decade^{-1}. Grey shading represents the statistical significance for the trends. See text for details on the linear trend and the statistical significance calculation.

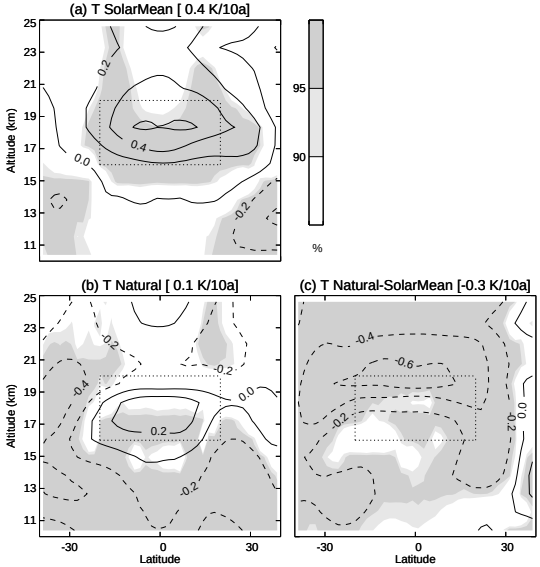

Figure 3. (a, b) Latitude-height sections of composite temperature trends over selected time periods (1958–1968, 2001–2011, 2045–2055, and 2089–2099, see Fig. 1) from the *Natural* and *SolarMean* runs, respectively; contour interval: 0.2 K decade^{-1}. **(c)** The differences between **(a)** and **(b)**. Grey shading represents statistically significant trends. See text for details on the calculation of the composite trend , and the testing of the statistical significance. The decadal temperature trend in the title is the mean value from the dashed box.

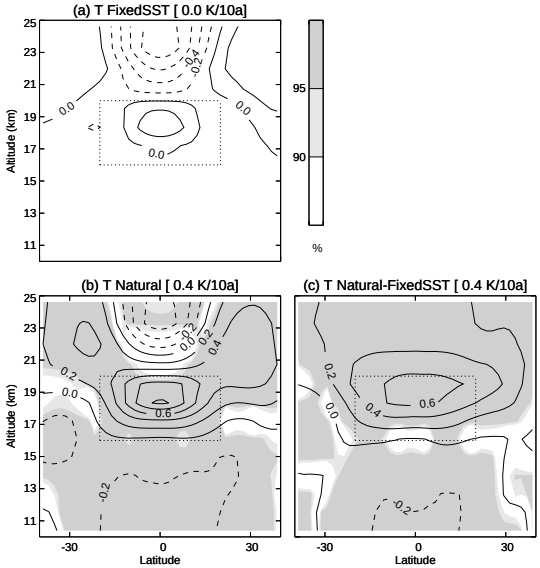

Figure 4. (a, b) Latitude-height sections of composite temperature trends over selected time periods (1956–1968, 1980–1991, 2001–2014, 2028–2043, 2047–2057, see Fig. 1) from the *Natural* and *FixedSST* runs, respectively; contour interval: 0.2 K decade^{-1}. **(c)** The differences between **(a)** and **(b)**. Grey shading as in Fig. 3.

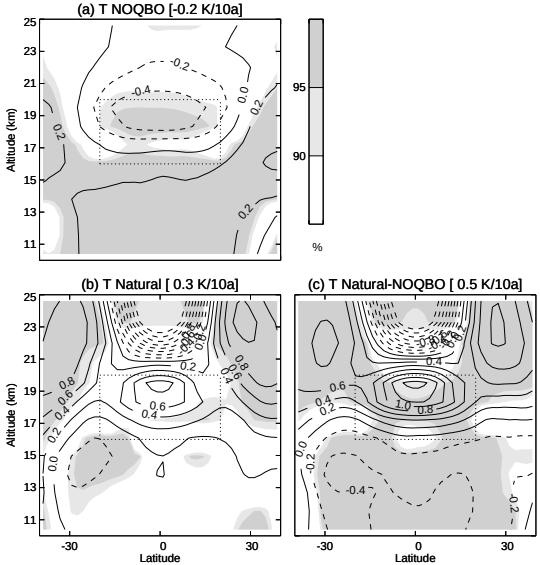

Figure 5. Same as Fig. 3, but for the impact of the QBO amplitude on temperature trends **(c)** by comparing the *Natural* and the *NOQBO* experiments **(a, b)** for the periods 2003–2017 and 2054–2068 (see Fig. 1); contour interval: 0.2 K decade^{-1}.

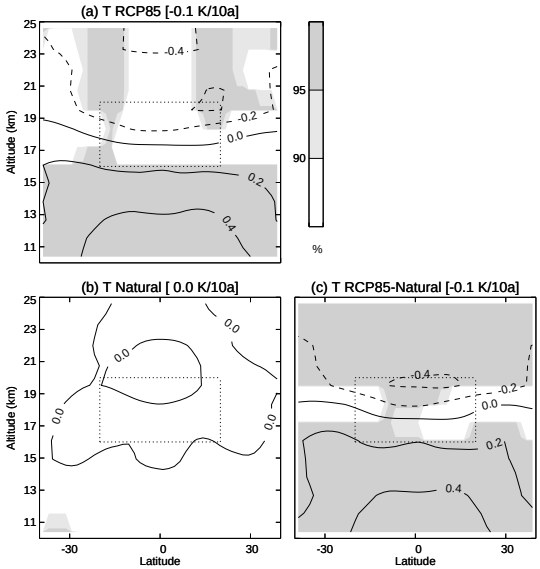

Figure 6. Same as Fig. 3, but for the impact of anthropogenic forcings (GHGs and ODS) on temperature trends by comparing the *Natural* and *RCP85* experiments **(a, b)** for the period 2001–2050; contour interval: 0.2 K decade^{-1}.

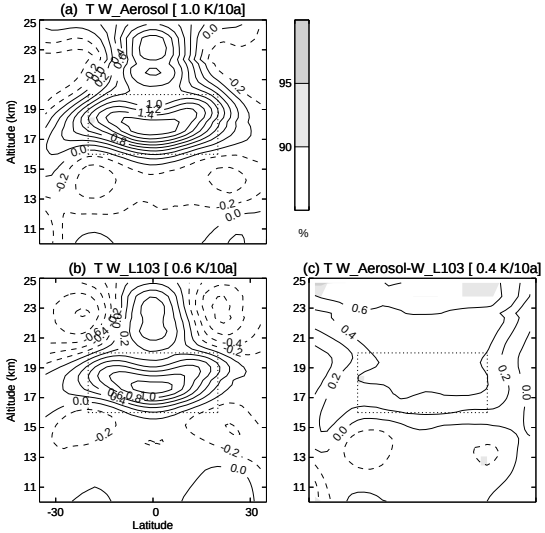

Figure 7. Same as Fig. 3, but for the impact of stratospheric aerosols on temperature trends by comparing the *W_L103* and the *W_Aerosol* experiment **(a, b)** for the period 2001–2010; contour interval: 0.2 K decade^{-1}. The temperature trends in the *W_L103* run were calculated by ensemble mean.

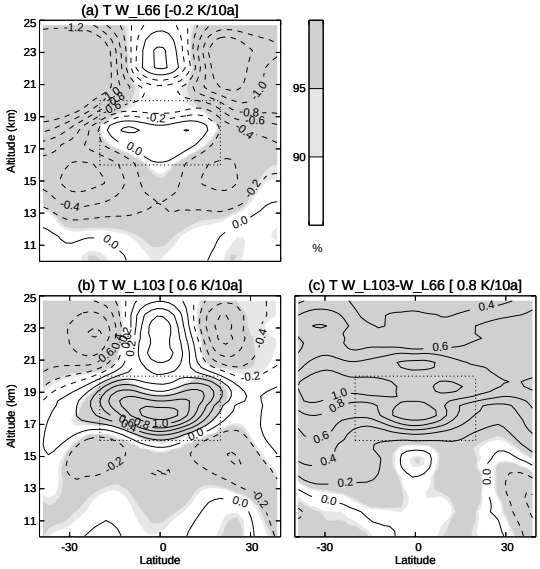

Figure 8. Same as Fig. 3, but for the impact of the differences in vertical resolution on temperature trends **(c)** by comparing the *W_L103* and *W_L66* experiments **(a, b)** for the period 2001–2010; contour interval: 0.2 K decade^{-1} and grey shading as in Fig. 3. The temperature trends in the *W_L103* and *W_L66* runs are calculated by multiple linear regression for the three ensembles.

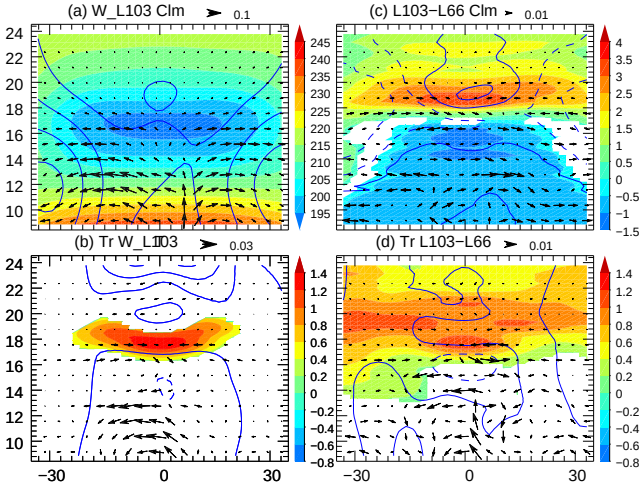

Figure 9. (a) Annual mean climatological zonal mean zonal wind (contours, contour interval 10 m s^{-1}, dashed lines indicate easterly winds), BDC vector (arrows, scaled with the square root of pressure) and temperature (colour shadings) for the *W_L103* experiment from 8 to 25 km and 35° S through 35° N. **(c)** Differences of the zonal mean zonal wind (contour interval 1.0 m s^{-1}), BDC vector and temperature (colour shadings indicate 95 % statistical significances) between the *W_L103* and the *W_L66* experiments. (**b** and **d**) Same as **(a)** and **(c)**, but for the linear trends from 2001 to 2010. The shadings in **(b)** and **(d)** indicate 95 % statistical significance. The contour intervals are 2 m s^{-1} and 1 m s^{-1} in **(c)** and **(d)**, respectively.